Using the hybrid DAS-SR method for damage localization in composite plates

Nokhbatolfoghahai, A.; Navazi, H. M.; Groves, R. M.

DOI
10.1016/j.compstruct.2020.112420

Publication date
2020

Document Version
Final published version

Published in
Composite Structures

Composite Structures 247 (2020) 112420

Contents lists available at ScienceDirect

Composite Structures

journal homepage: www.elsevier.com/locate/compstruct

Using the hybrid DAS-SR method for damage localization in composite plates

A. Nokhbatolfoghahai[a], H.M Navazi[a,*], R.M. Groves[b]

[a] Department of Aerospace Engineering, Sharif University of Technology, Azadi Ave., PO Box: 11155-8639, Tehran, Iran
[b] Aerospace Non-Destructive Testing Laboratory, Faculty of Aerospace Engineering, Delft University of Technology, 2628 CD Delft, The Netherlands

ARTICLE INFO

Keywords:
SHM
Composite structure
Lamb waves
Barely Visible Impact Damage (BVID)
Sparse reconstruction
Delay-and-Sum

ABSTRACT

In this paper, the hybrid Delay-And-Sum (DAS) with Sparse Reconstruction (SR) method was further developed for damage location in composite plates. In composite materials, anisotropy leads to some challenges in using conventional damage location methods, which are developed for isotropic materials. In the hybrid DAS-SR method, the DAS and SR methods were combined as a complement of each other. To investigate the DAS-SR method for composite structures, the group velocity of the travelling wave for different directions was first measured experimentally via PZTs. The DAS and SR formulations were then modified to be compatible with the direction-dependent group velocities. The results show that this modification increases the accuracy of the DAS and SR methods for damage location in a composite plate. However, using group-velocity instead of phase-velocity in the standard SR method, causes some model mismatch and errors in the damage localization and this problem was solved by using the modified hybrid DAS-SR method. The experimental results demonstrated that the performance of the modified hybrid method for detection and location of barely visible impact damages as well as for multi-location artificial damages is better than that of the DAS and SR methods when separately used.

1. Introduction

Composite structures are widely used in aerospace, civil and other industries to reach lighter weight, higher operating temperatures, greater stiffness, higher reliability and increased affordability [1]. In aerospace structures, Carbon fiber-reinforced plastics (CFRPs) are the most common composite and they are becoming more and more prevalent [2]. For instance, in civil aircraft from 1980 to 2015 the composite content by weight increased from 5 to 6% to 35–50% and this increasing trend in the usage of composite materials is also expected in the future [1]. The extensive use of composite materials in aircraft structures increases the demand for non-destructive evaluation for damage detection and integrity assessment of composite structures. Unlike in metallic structures where damage occurs mostly due to fatigue cracks, in composite materials damage occurs in many more ways such as delamination, matrix cracking, fiber failure and fibre-matrix debonding and the prediction of damage behavior is much more complex than in metallic structures [3]. In addition, composite structures are vulnerable to Barely Visible Impact Damages (BVID) caused by low energy impacts such as tool drop, runway debris, bird strike, etc. Such damages may go undetected during visual inspection, but could potentially grow during aircraft operation and eventually cause structural failure. As a result, Structural Health Monitoring (SHM) for composite structures receives a lot of attention as a way to monitor composite structures in-service. In addition to potential safety improvements, SHM can significantly reduce maintenance costs by replacing the scheduled maintenance by condition-based maintenance [4].

The basic tasks of SHM systems are damage detection and location. For NDT inspections, among the different methods used, ultrasonic waves has been a reliable and accepted method for over a half century [5]. Also, to perform ultrasonic damage location in plate-like structures, using guided waves is an attractive method because of the compromise between sensitivity to damage, extent of the area monitored and the price, additional weight and time for implementation [6]. In composite structures, material anisotropy leads to the dependence of the group and phase wave velocity on the direction of propagation and layup configuration. There is also an angle between the group velocity and phase velocity vectors [7]. These phenomena cause some challenges in using Lamb waves for composite structures.

Working on the application of Lamb waves in composite structures began in the late 1980s and early 1990s at NASA [8] by Saravanos [8–10]. Detection of fatigue and thermal damage in composites were separately investigated by Seale et al. [11]. Guo and Cawley investigated the interaction of the S0 mode of a Lamb wave with

* Corresponding author.
E-mail address: navazi@sharif.edu (H.M. Navazi).

https://doi.org/10.1016/j.compstruct.2020.112420
Received 9 December 2019; Received in revised form 15 April 2020; Accepted 24 April 2020
Available online 29 April 2020

delamination in composite laminates and they showed the high dependency of the reflected wave to the position of the delamination through the thickness of the laminate [12]. In addition to damage detection, many researchers focused on damage localization methods to locate failures quickly and efficiently. Various imaging methods based on guided Lamb waves have been developed for this purpose including tomography [13,14], phased array techniques [15–17], methods based on neural networks [18,19], and sparse array methods [20–24]. Among these methods, sparse array imaging is attractive due to its low cost and ease of implementation, as well as its capability of seeing damage from different angles [5,21,25].

Among the sparse array-based methods, the Delay-and-Sum (DAS) method is the most commonly used method due to its robustness and conceptual simplicity. This method was developed by Wang et al. at in 2004 [23] and Michaels (2008) [26] has successfully utilized this method to locate a notch and corrosion on an aluminum plate. However, the performance of this method tends to be poor in the presence of multiple damages or in complex structures [27]. Also, Sharif-Khodaei and Aliabadi evaluated the applicability of the DAS algorithm for damage detection in aluminum and composite plates and they also further developed this method by proposing the windowed energy arrival method (WEAM). Their work showed in both cases, that their proposed method was successful in detecting the damage, but there was some errors in localizing the damage in the complex composite plates with a stiffener [28,29]. Zeng et al. proposed a damage localizing method for composite structures based on the delay and sum method that considers multipath scattering from boundary conditions in the structure and that could successfully detect and locate an added mass on the specimen as an artificial damage with a single pair of transducers [30].

In 2013 Levine and Michaels [31] developed an imaging method that is based on sparse reconstruction (SR) and in some cases, the images reconstructed via this method have been shown to be superior to the conventional DAS [31]. Furthermore, as this method is a dictionary-based method it could act as an adaptive method and some structural complexities (such as direction-dependent wave velocity in composites) could potentially be modeled in its pre-computed dictionary matrix. Despite all these advantages, this method has some challenges with robustness. In images reconstructed via the SR method, the spot size is typically one or two pixels, however, detection can completely fail in the presence of multiple damages or in complex structures [5].

In this paper, we extend our work in hybrid DAS-SR to the problem of damage localization in anisotropic materials by using direction-dependent time of flight calculated in the DAS part and in the dictionary matrix formulation for SR. In this paper we demonstrate the performance of these new signal processing methods by experimental testing and analysis.

2. Theoretical background

In this section, the mathematical formulation of the Lamb wave propagation, the SR method, the DAS method and the hybrid DAS-SR method are presented for composite plate-like structures.

2.1. Lamb wave signal

Lamb waves are guided elastic waves that propagate in plate-like structures. They were first described by Horace Lamb in 1917 [32]. Propagating Lamb waves have three mode types, symmetric modes (S_n) and antisymmetric modes (A_n) which propagate in the plane perpendicular to plate and shear-horizontal (SH_n) which propagate in the plane of the plate. In anisotropic materials, unlike metals, the phase and group velocities are direction-dependent due to the directional material properties of composites [30,33,34]. Also, in an anisotropic material there is an angle between the group and phase velocity vectors as shown in Fig. 1.

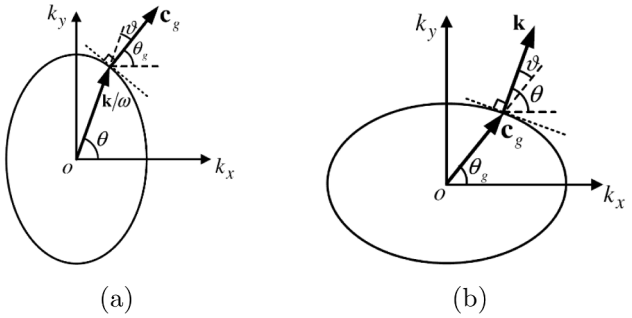

Fig. 1. Schematic of geometric relation between wave vector and group velocity vector: (a) slowness curve; (b) wavefront curve [34].

In Fig. 1, c_g and θ_g are magnitude and angle of the group velocity respectively, $\mathbf{k} = [k_x, k_y]$ is the wave number that points the direction of propagation and θ is the direction of wave propagation and ϑ is the skew or steering angle [34]. Using free software LAMSS-COMPOSITES V1.0 downloaded from [35], dispersion curves for a cross-ply CFRP composite with a layup of $[0/90/0/90]_S$ and material properties presented in [35] were achieved for waves traveling along the directions 0° and 45°, The dispersion curves are presented in Fig. 2.

In guided wave based SHM systems which use a sparse-array configuration of PZTs, a typical operation consists of generating Lamb waves via each transducer in turn while the others record the response, until a full measurement set of pairwise signals is acquired [27]. Most SHM imaging algorithms operate on signal differences, so pre-recorded baseline signals are subtracted from measurements to create a set of residual signals to detect changes, due to damage or other effects [31]. To calculate differential signals, here, individual signals are scaled based upon the amplitude of the direct arrival from a corresponding transducer pair and reduced by the square root of the propagation distance as in [26]. The residual signal $R_{s,r}(t)$ is obtained by subtracting the scaled baseline signal $\hat{S}^b_{s,r}(t)$ from the scaled measured signal $\hat{S}_{s,r}(t)$.

$$R_{s,r}(t) = \hat{S}_{s,r}(t) - \hat{S}^b_{s,r}(t) \tag{1}$$

To separate the amplitude and phase characteristics of these signals and to compensate for the effect of phase difference due to model mismatch, the envelope-detected residual signal, $y_{s,r}(t)$ for each pair of actuator "s" and receiver "r" is used. It is obtained from the Hilbert transform as:

$$y_{s,r}(t) = abs(Hilbert(R_{s,r}(t))) \tag{2}$$

where $y_{s,r}(t)$ is the input to both the DAS, SR and hybrid algorithms described below.

2.2. DAS imaging method

To perform the DAS method, the time of flight (TOF) of a wave propagating from actuator "s", received at location (x, y) and scattered back to the sensor "r" is calculated for all pairs of transmitters. In this work to generate an image of the structure via the DAS method, we have used the formulation presented in [26]. The value $E(x, y)$ of each location in the image is then obtained as follows:

$$E(x, y) = \frac{1}{N(N-1)} \sum_{s=1}^{N-1} \sum_{r=1}^{N} y_{s,r}(t_{sqr}(x, y)) \tag{3}$$

where, N is the number of transducers and $t_{sqr}(x, y)$ is the calculated time-of-flight based on measured group velocity for the wave that is transmitted by PZT "s" received to point q at location (x, y) then scattered and received by PZT "r". To adjust Eq. (3) to be valid for an anisotropic material with directional-dependent group velocity $C_g(\theta)$, $t_{sqr}(x, y)$ is calculated as follows:

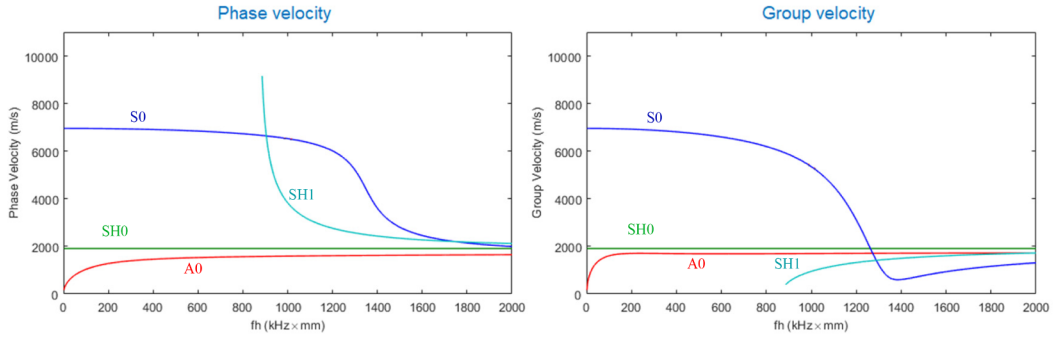

(a)

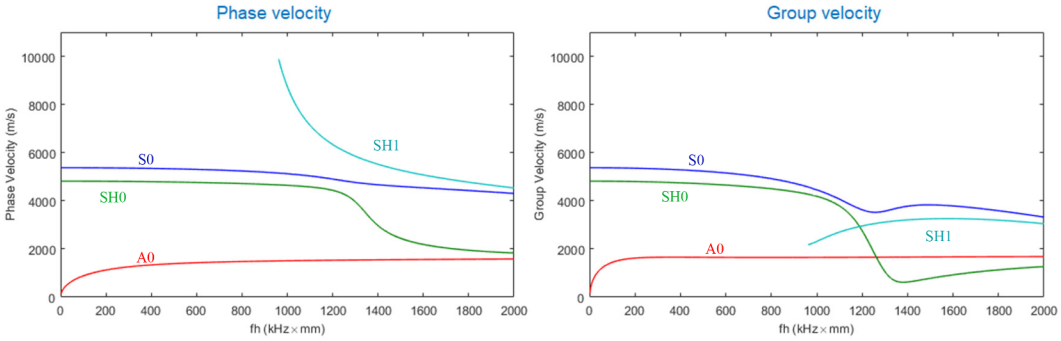

(b)

Fig. 2. Dispersion curves of Lamb waves traveling (a) along $\theta = 0^{\circ}$ (b) along $\theta = 45^{\circ}$ where fh is the frequency multiplied by the plate thickness.

$$t_{sqr}(x, y) = \frac{\|\vec{q} - \vec{s}\|_2}{C_g(\theta_{s,q})} + \frac{\|\vec{r} - \vec{q}\|_2}{C_g(\theta_{q,r})} \tag{4}$$

In Eq. (4), C_g is constant for a specific angle θ, $\theta_{a,b} = \angle(\vec{b} - \vec{a})$ and $||\ ||_2$ denotes the l_2-norm of a vector.

2.3. The sparse reconstruction method

Sparse reconstruction (SR) refers to dictionary based techniques for solving the linear underdetermined inverse problem $\mathbf{y} = \mathbf{Ax}$ to calculate an unknown sparse vector $\mathbf{x}$, using the known vector $\mathbf{y}$ and the dictionary matrix $\mathbf{A}$. In an SHM system, the SR method mainly uses the sparsity assumption of structural damages [5]. In this method, to reconstruct an image of a structure the residual signal is assumed to be composed of a linear combination of signals from individual scattering points as [31]:

$$y_{s,r}(t) = \sum_{q=1}^{p} x_i a_{s,q,r} \tag{5}$$

where x_i is the unknown coefficient that shows the possibility of damage presence in the pixel "q". Also, the $a_{s,q,r}$ is the analytically computed signal that roughly estimates the shape of the scattering wave due to the interaction of Lamb-wave propagated from point "s" with a scatterer located at point "q" and then received by a sensor placed at point "r". In anisotropic materials, to calculate $a_{s,i,r}$ analytically it is required to calculate the dispersion curve in different directions. However, in many cases, since the exact material properties of a composite structure in operating conditions is not available, it is not possible to analytically calculate the dispersion curves of the composite plate with an acceptable accuracy to be applicable in damage detection algorithms. In addition, in [34] the comparison between the dispersion curves for a composite plate achieved from experimental and analytical formulation, showed that at some frequencies there is about a 10% difference between the results which is not acceptable for damage localization algorithms. In this study, we assume the dispersion curves are not available from literature and we have used an upgraded dictionary generation method in which group velocity is calculated from experimental data in different wave propagation directions. Also, by using calculated direction-dependent group velocities, the shape of the envelope-detected excitation signal $x'(t)$ after traveling a distance "d" in θ direction can be roughly estimated as:

$$a(t, \theta) = \left(\frac{d}{d_{ref}}\right)^{-\frac{1}{2}} \int_R X'(f) e^{i2\pi f\left(t - \frac{d}{C_g(\theta)}\right)} df \tag{6}$$

Eq. (6), which is used instead of Eq. (1) in [31], shows a simple time shifting equal to a time of flight $T_0 = \frac{d}{C_g(\theta)}$ in the envelope-detected excitation signal $x'(t)$. Also, $X'(f)$ is the Fourier transform of $x'(t)$, $i = \sqrt{-1}$ and d_{ref} is an arbitrary reference distance. It should be noted in the calculation of group velocity in Eq. (6), that the dispersive characteristic of the Lamb wave is neglected. So, to form the dictionary matrix the estimated shape of propagating Lamb waves are considered. Using these assumption, a wave that is excited at point "s", which interacts with damage at point "q" and is then received by a sensor at point "r" could be described as

$$a_{s,q,r}(t) = \left(\frac{\|\vec{r} - \vec{q}\|_2 . \|\vec{q} - \vec{s}\|_2}{d_{ref}^2}\right)^{-\frac{1}{2}} \int_R \left\{ H(f, \theta_{s,q}, \theta_{q,r}) . X'(f) . e^{\frac{-i2\pi f \|\vec{q} - \vec{s}\|_2}{C_g(\theta_{s,q})}} . e^{\frac{-i2\pi f \|\vec{r} - \vec{q}\|_2}{C_g(\theta_{q,r})}} \right\} e^{i2\pi ft} df \tag{7}$$

where $H(f, \theta_{s,q}, \theta_{q,r})$ describes the interaction of the Lamb wave with damage and due to unknown prior information about the type of damage, this value is set equal to 1. The decomposition can be done for all pairs of actuator-sensors and for a distributed array of N transducers

the linear equation $\mathbf{y} = \mathbf{A}\mathbf{x}$ is formed as:

$$\underbrace{\begin{bmatrix} y_{1,2}(t) \\ y_{1,3}(t) \\ \vdots \\ y_{a,r}(t) \\ \vdots \\ y_{N,N-1}(t) \end{bmatrix}_{N(N-1)}}_{\mathbf{y}} = \underbrace{\begin{bmatrix} a_{1,1,2} & a_{1,2,2} & \cdots & a_{1,q,2} & \cdots & a_{1,p,2} \\ a_{1,1,3} & a_{1,2,3} & \cdots & a_{1,q,3} & \cdots & a_{1,p,3} \\ \vdots & \vdots & \ddots & \vdots & \ddots & \vdots \\ a_{a,1,r} & a_{a,2,r} & \cdots & a_{a,q,r} & \cdots & a_{a,p,r} \\ \vdots & \vdots & \ddots & \vdots & \ddots & \vdots \\ a_{N,1,N-1} & a_{N,2,N-1} & \cdots & a_{N,q,N-1} & \cdots & a_{N,p,N-1} \end{bmatrix}_{[N(N-1)]p}}_{A} \underbrace{\begin{bmatrix} x_1 \\ x_2 \\ \vdots \\ x_q \\ \vdots \\ x_p \end{bmatrix}_p}_{\mathbf{x}} \tag{8}$$

where $\mathbf{A}$ is the dictionary matrix, $\mathbf{y}$ is the envelope-detected residual signals and the unknown vector $\mathbf{x}$ shows the location of damages that is assumed to be sparse.

In this study, to solve the linear inverse problem, the Basis Pursuit Denoising (BPDN) method which is an l_1-optimization method is used (see Levine [5] and Levine and Michaels [27,31]). This method minimizes the l_1-norm of the vector$\mathbf{x}$ to solve the optimization problem as:

$$\mathbf{x} = \text{argmin}\|\mathbf{x}\|_1 \text{subjectto} \|\mathbf{y} - \mathbf{A}\mathbf{x}\|_2 < \sigma \tag{9}$$

where σ is the user-specified parameter that acts as a trade-off parameter between sparsity and reconstruction accuracy.

2.4. Hybrid DAS-SR method

A simple comparison of the DAS and SR methods shows that in some conditions the robustness of the DAS method is higher than the SR method; however, its accuracy is less than SR. In the case of composite materials, the accuracy of DAS images may further decrease with a large estimated damage location size due to the use of imprecisely known group velocities; however, the detection by the SR method in some cases may totally fail due to model mismatch and rough estimation due to the use of group velocity instead of phase velocity in the forming dictionary matrix [5]. Therefore, it seems that in composite materials these two methods could complement each other, as they have been demonstrated to do in isotropic materials [36]. In the hybrid DAS-SR method the DAS result is applied to the SR method as the prior support information. To use a hybrid DAS-SR method, we need to first define a prior support estimate $T \subset \{1, \cdots, p\}$, define weights for each pixel of the structure, and then solve the weighted l_1 minimization

$$\mathbf{x} = \text{argmin}\|\mathbf{x}\|_{1,\vec{w}} \text{ subject to } \|\mathbf{y} - \mathbf{A}\mathbf{x}\|_2 < \sigma \tag{10}$$

where $\|\mathbf{x}\|_{1,\vec{w}}$ is the weighted l_1-norm and is calculated as.

$$\|\mathbf{x}\|_{1,\vec{w}} = \sum_{i=1}^{n} w_i \ |x_i| \quad \text{and} \quad w_i = \begin{cases} w \in [0, 1] & i \in \tilde{T} \\ 1 & i \in \tilde{T}^c \end{cases} \tag{11}$$

In Eq. (11) lower weights are applied to the pixels with a higher probability of being nonzero. To define the support set $T = \{T_1, \cdots, T_i\}$ we define $\widehat{E}_i = \frac{E_i}{Max(E)}$ achieved by the DAS method for each pixel and set the threshold C_0 and we have:

$$T_i \in \{1, \cdots, p\} \quad \text{for} \quad i = 1, \ \cdots, p \quad \text{Where} \quad |E_i| > C_0 \tag{12}$$

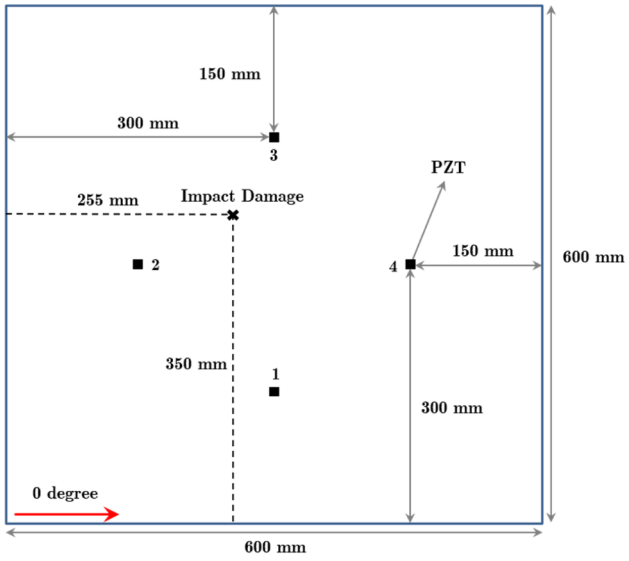

Fig. 3. Configuration of the plate with PZT transducers and impact damage.

To define the weights w_i for each pixel, here we use the results achieved by DAS and propose the following relationship:

$$w_i = \frac{1 + \exp(1)}{1 + \exp(1 + 10\widehat{E}_i)} \tag{13}$$

Eq. (13) is an empirical relationship that, in addition to applying prior support information can have two other advantages including: 1) approach the l_1-norm of the sparse vector $\mathbf{x}$ to l_0-norm and consequently increase the computational speed and reduce the level of noise [37]; 2) decrease the correlation between columns of dictionary matrix $\mathbf{A}$ to increase the accuracy of recovery of vector $\mathbf{x}$. The general form of Eq. (13) was determined based on [37] in which, Mohimani et al. showed that the exponential function can estimate the l_0-norm of the vector. Considering that, we define Eq. (13) based on the exponential function, which could eventually approach the sparse reconstruction to the l_0-norm minimization. Also, to determine the coefficients, an optimization could be performed on the correlation of the columns of matrix $\mathbf{A}_{\boldsymbol{w}}$ which is obtained as:

$$\mathbf{A}_{\boldsymbol{w}} = \boldsymbol{A} \times \boldsymbol{diag}(\vec{\boldsymbol{w}}) \tag{14}$$

By considering the above and also various cases with several conditions and some mathematical techniques presented in [38,39] the relationship for defining weights was empirically determined as shown in Eq. (13).

3. Case study

In order to perform an experimental test on a composite structure, two carbon-fibre epoxy composite plates, with cross-ply and quasi-isotropic layup, were manufactured. In the quasi-isotropic plate, eight unidirectional prepreg plies from M21/T800 were used with a layup of $[45/-45/0/90]_S$, and the cross-ply plate manufactured using twelve unidirectional prepreg plies from AS4/8552 were used with a layup of $[0/90]_{3S}$. The thickness of both plates after thermal curing was about

Table 1
Material properties of prepregs [40].

	UD tensile strength (MPa)	UD tensile modulus (GPa)	UD compressive strength (MPa)	UD compressive modulus (GPa)	45° in-plane shear strength (MPa)	45° in-plane shear modulus (GPa)
T800/M21	2451	171	1231	148	145	5.1
AS4/8552	2205	141	1530	128	128	5.6

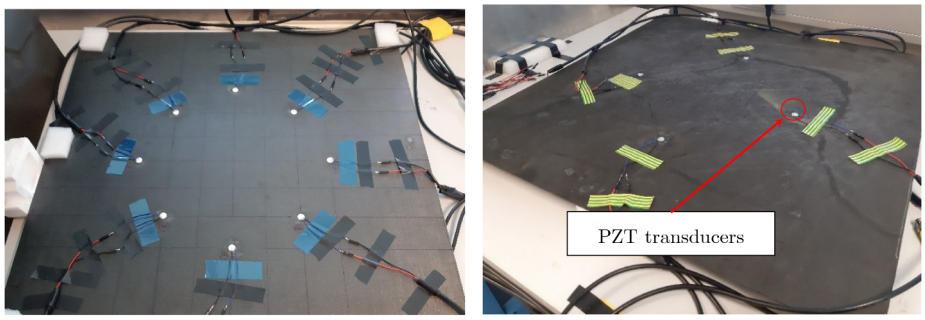

Fig. 4. Manufactured composite plates with the bonded PZTs (A) cross-ply plate (B) quasi-isotropic plate.

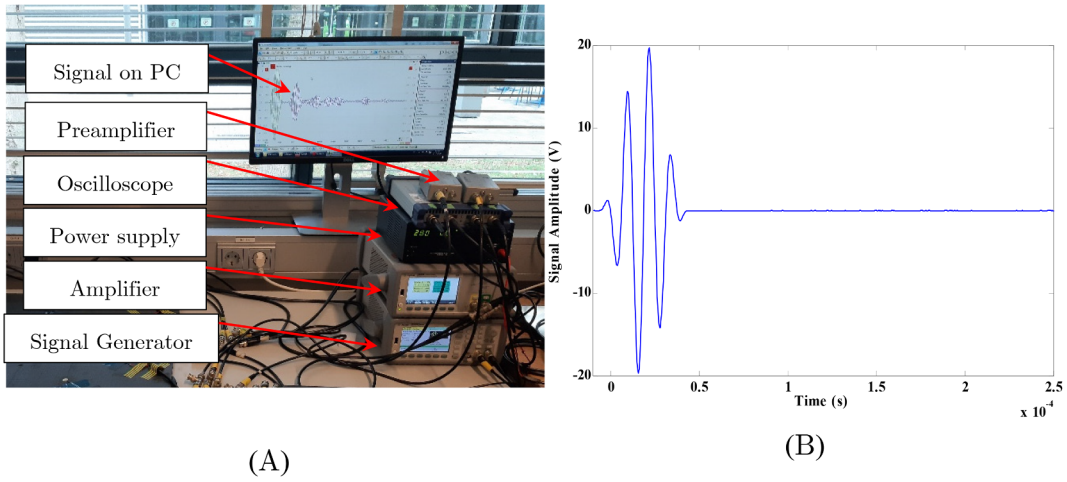

Fig. 5. (A) Experimental setup for data generation and acquisition (B) The excitation signal as an input to signal generator.

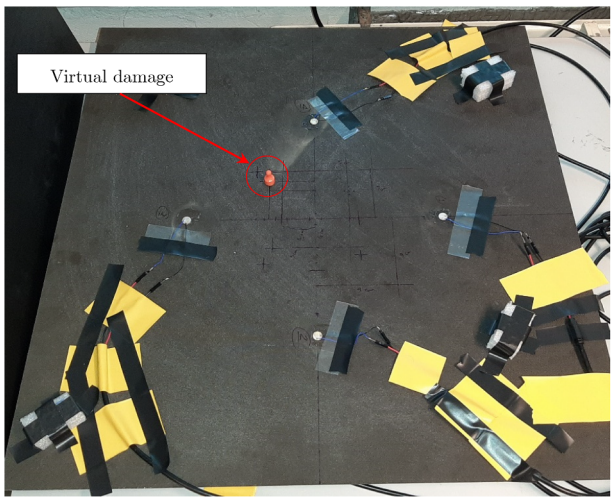

Fig. 6. The composite plate with an attached magnet as a virtual damage.

Fig. 7. The impact tower used for the impact test.

2.15 mm and the dimensions of the final product was 60 cm by 60 cm. The material properties of the prepreg used are shown in Table 1.

Also, to generate and detect Lamb waves, circular PZT transducers were used on both sides of the plate to generate and detect pure A0 and S0 modes. Fig. 3 shows the configuration of the plate with the PZTs and the zero degree fibre orientation.

Fig. 4 shows both manufactured plates with the bonded PZT transducers. It should be noted, although in Fig. 4 (A) we have attached eight double-side PZTs on the cross-ply plate, in this study we have switched off four of them to be comparable with the configuration shown in Fig. 3.

3.1. Experimental setup

Experimental tests were performed on the manufactured composite plate at the Non-Destructive Testing Laboratory of TU Delft. The PZTs

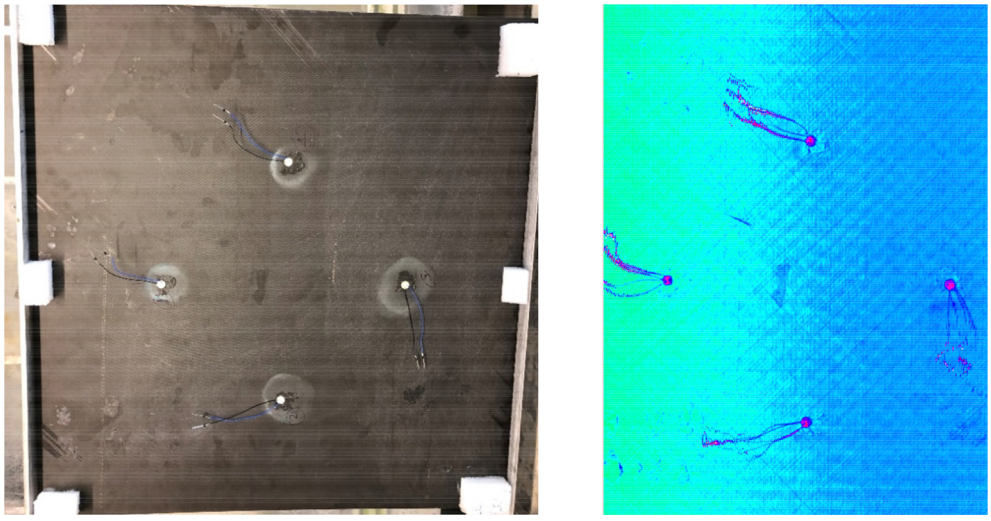

Fig. 8. The C-scan result of composite plate after impacted by 8.7 J energy.

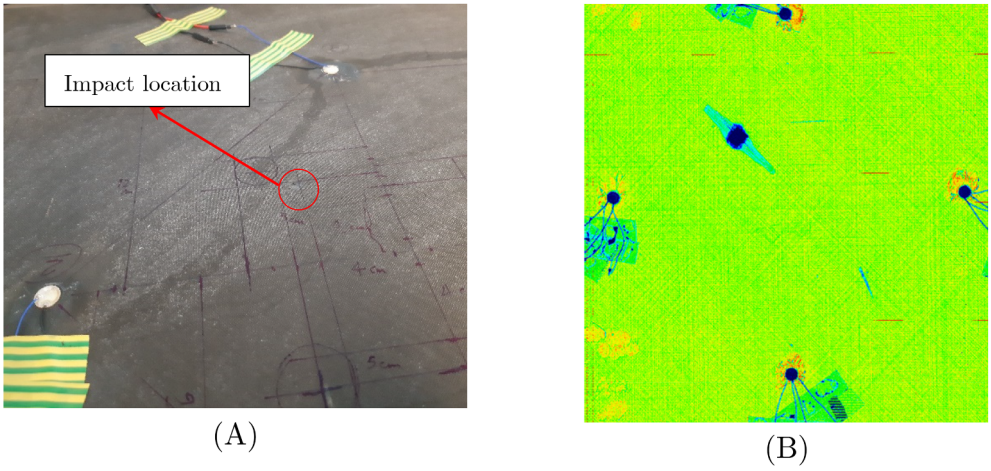

Fig. 9. The composite plate after second impact (A) Impact damage on the plate (B) C-scan image of impacted plate.

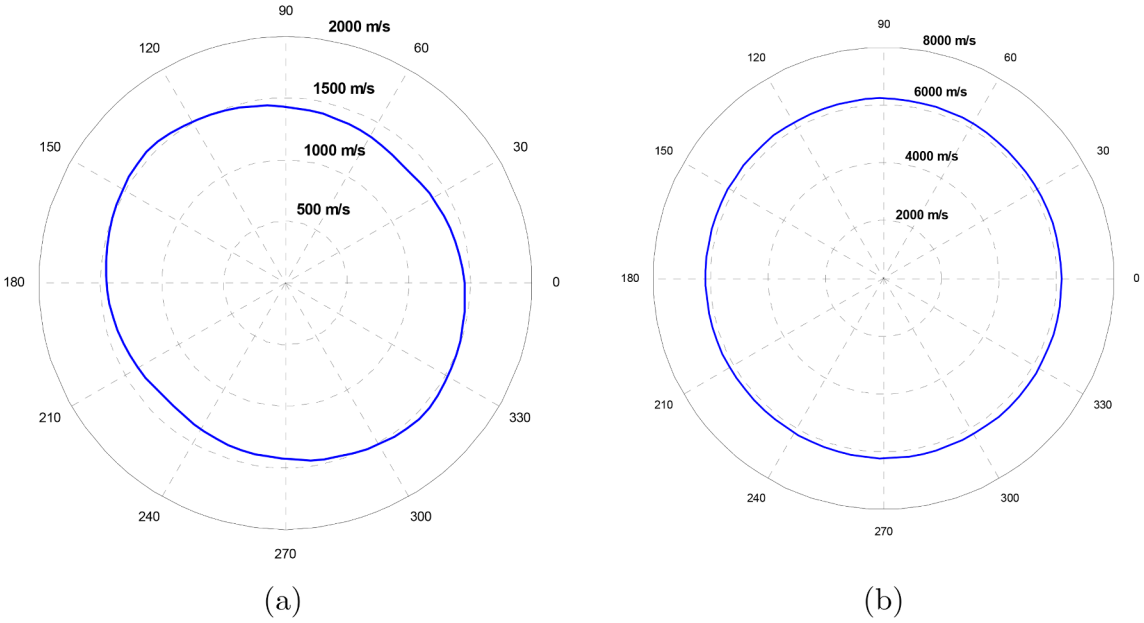

Fig. 10. Group velocity of Lamb wave propagated in the quasi-isotropic plate measured from experimental data in different directions for (a) A0 Mode (b) S0 Mode.

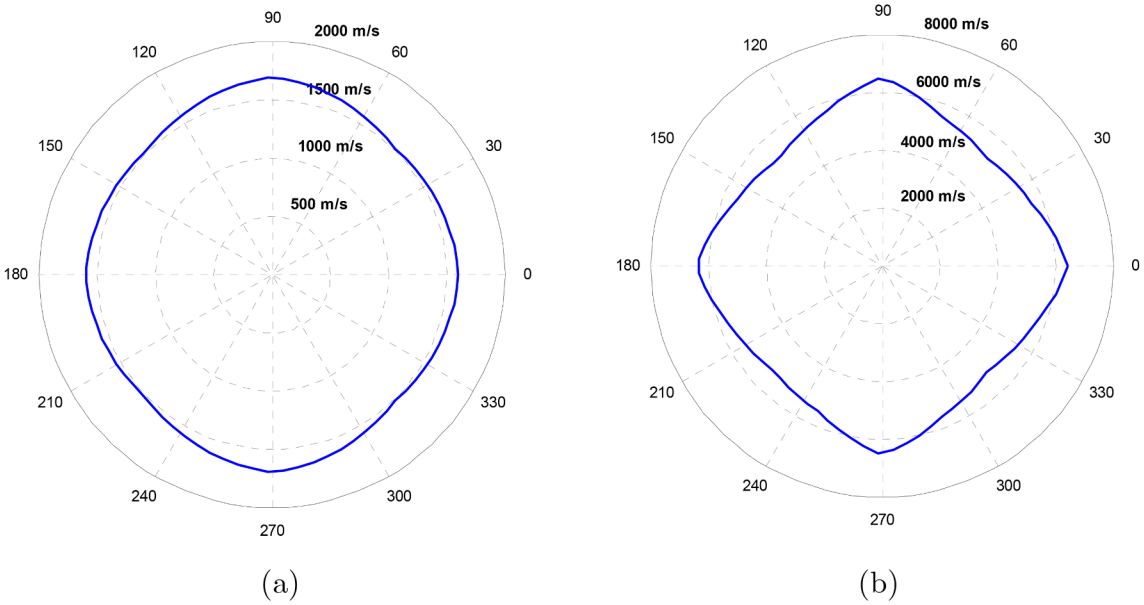

Fig. 11. Group velocity of Lamb wave propagated in the cross-ply plate measured from experimental data in different directions for (a) A0 Mode (b) S0 Mode.

Table 2
Group wave velocity measured in different directions.

Angle	Path	Quasi-isotropic plate		Cross-ply plate	
		S_0 Mode (ms^{-1})	A_0 Mode (ms^{-1})	S_0 Mode (ms^{-1})	A_0 Mode (ms^{-1})
0°, 180°	$PZT_{2\to4}$	6178	1451.6	6422	1601
45°, 225°	$PZT_{1\to4}$ $PZT_{2\to3}$	6160	1343.2	5188	1512
90°, 270°	$PZT_{1\to3}$	6230	1428.9	6521	1701
135°, 315°	$PZT_{1\to2}PZT_{4\to3}$	6234	1554.9	5124	1512

used for generating Lamb waves were type PIC 255 from PI company with 10 mm diameter and 0.5 mm thickness, which were installed on the composite plate with superglue after surface cleaning. For Lamb wave generation, a 90 kHz four-cycle Hann windowed tone burst with a peak-to-peak voltage of 8 V was generated by an Agilent 33500B waveform generator and amplified by a wideband voltage amplifier (Agilent 33502A) to give a 40 V peak-to-peak excitation voltage. The excitation frequency was selected based on the lower attenuation, not exciting higher order modes and to allow the difference between the velocity of S0 and A0 mode to be distinguishable. A PicoScope 6402 was used to capture the received signals from the PZTs and a wideband preamplifier MISTRAS 2/4/6C was used to amplify the received signals. The experimental setup and the excitation signal are shown in Fig. 5.

3.2. Virtual and impact damage

To verify the methods discussed in section 2, first single and multiple-virtual damages were simulated with small magnets with a diameter of 10 mm, affixed to both sides of the both plates. Fig. 6 shows the simulated damage on the quasi-isotropic plate.

At the next step the quasi-isotropic plate was impacted at two

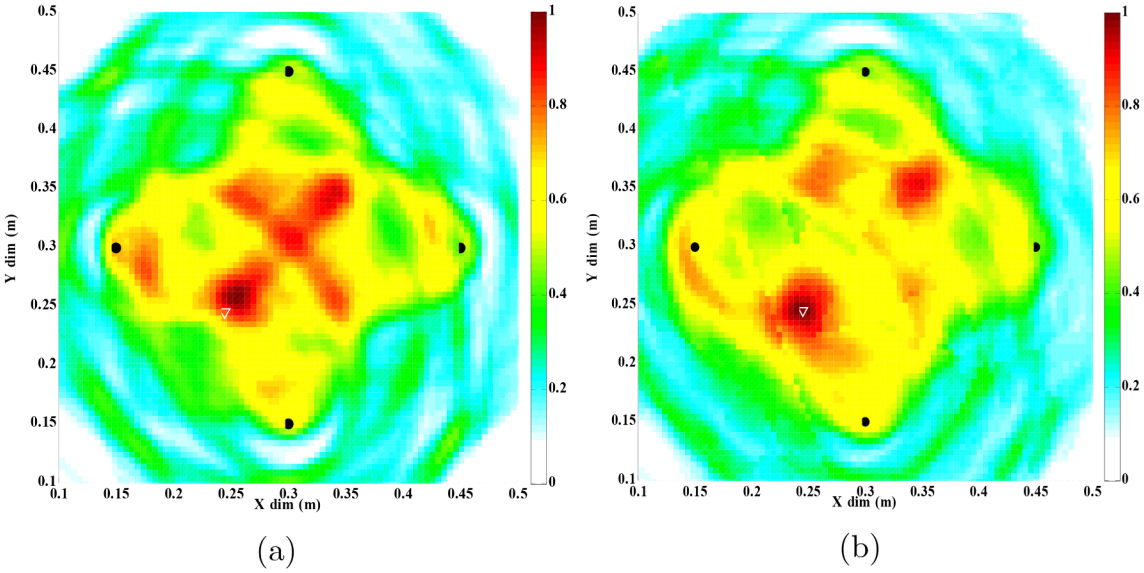

Fig. 12. Images reconstructed via (a) the conventional DAS method (b) the modified DAS Method for the quasi-isotropic plate. Black circles denote the PZTs and the triangle shows the damage location coordinate (25 cm, 25 cm).

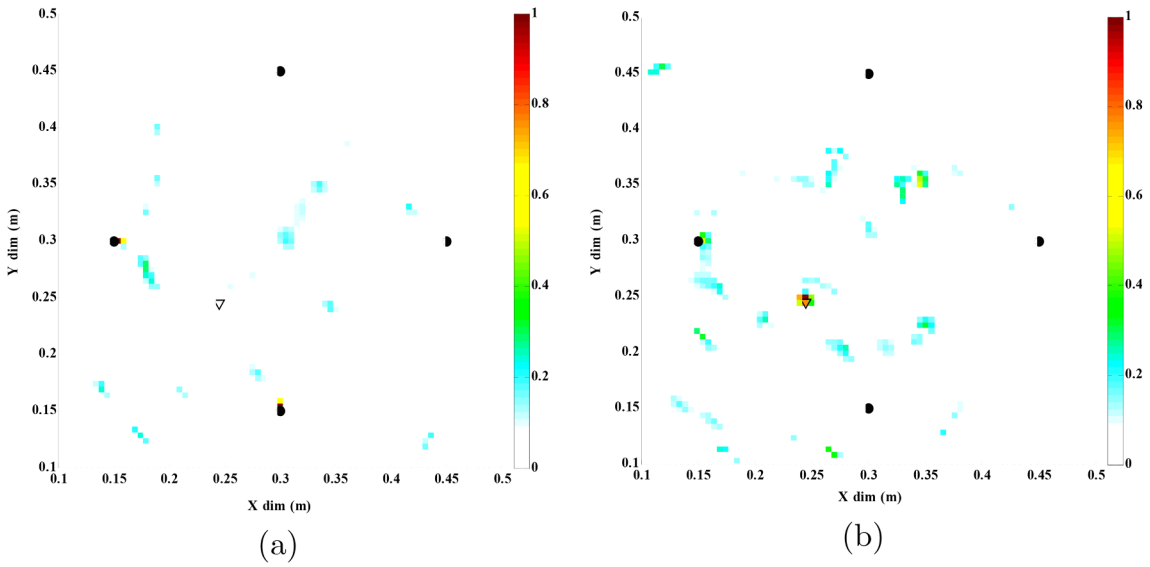

Fig. 13. Images reconstructed via (a) the conventional SR method (b) the modified SR Method for the quasi-isotropic plate. Black circles denote the PZTs and the triangle shows damage located at coordinate (25 cm, 25 cm).

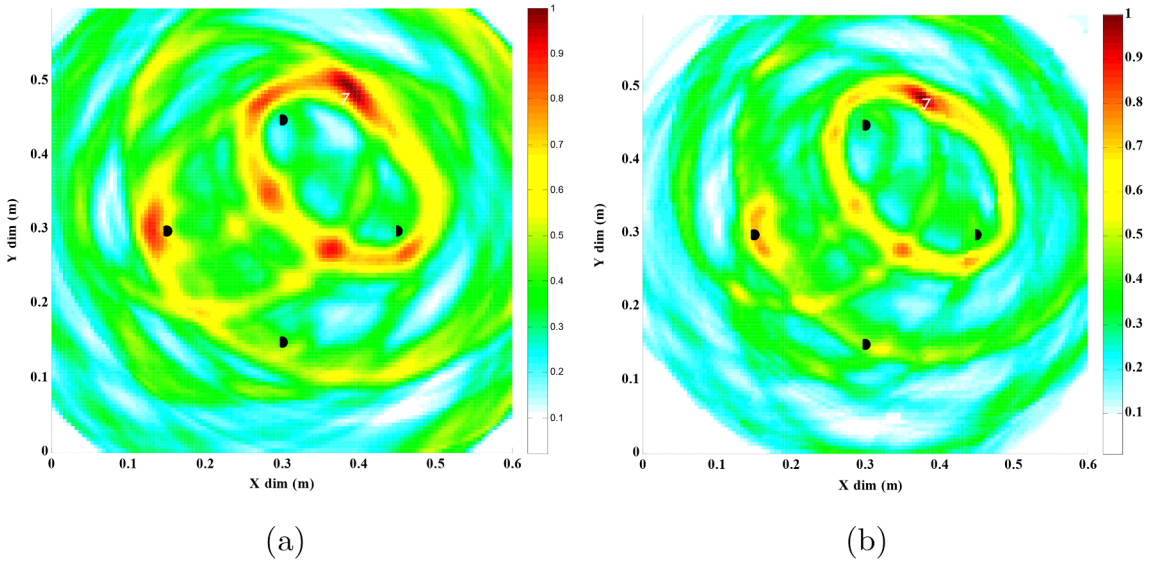

Fig. 14. Images reconstructed via (a) the conventional DAS method (b) the modified DAS Method for the cross-ply plate. Black circles denote the PZTs and the triangle shows the damage location coordinate (38 cm, 48 cm).

energy levels using an impact tower to induce damage. The first impact energy was 8.7 J (2.2 kg, 2.81 ms^{-1}) and the impactor was semi-spherical with a radius of 10 mm according to the standard equipment available in the laboratory. The impact tower is shown in Fig. 7. Fig. 8 shows the post-impacted plate and the C-scan result of the composite plate after the 8.7 J energy impact.

As is can be seen from Fig. 8 the impact did not create a detectable damage on the plate. As a result, the energy of the second impact at the same location was increased to 11.6 J (1.972 kg, 3.43 ms^{-1}) with an 8 mm semi-spherical impactor. Fig. 9 shows the impact effect and the C-scan image of the composite plate after the second impact

As is shown in Fig. 9(A) the impact damage is barely visible using visual inspection. However, the C-scan image depicted in Fig. 9(B), indicates the location of impact damage on the plate, and considering the C-scan image, the diameter of the main area of the damage is estimated to be 14 mm, approximately.

4. Results

In this section, the results obtained by the modified DAS and SR methods as well as the hybrid DAS-SR method are presented for the composite plate with two and three virtual damages and for one impact damage location. It should be noted that, as the A_0 mode is more sensitive to surface scatters [7] (such as surface attached magnets) we have used the A_0 mode for virtual damage detection. Also we have used the S_0 mode for impact damage detection because it is better in the detection of defects inside the thickness [7].

4.1. Wave velocity in different directions

To perform modified DAS and SR the first task was to calculate the group velocity in different directions from direct waves propagating between PZTs. For instance to calculate wave velocity at an angle of 45°, the direct propagated waves between PZT 1,2 and PZT 4,3 are used.

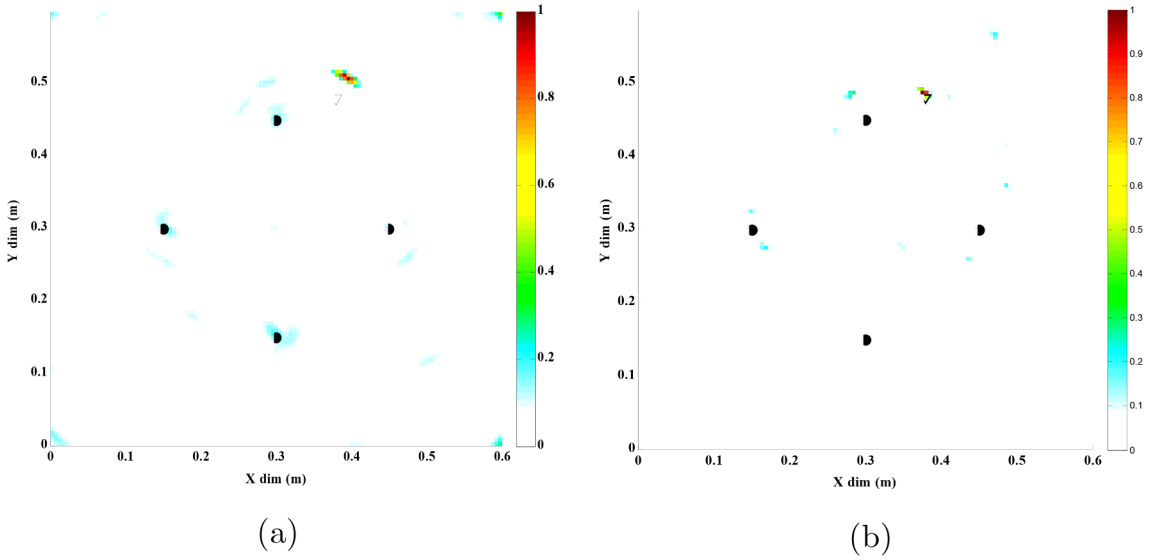

Fig. 15. Images reconstructed via (a) the conventional SR method (b) the modified SR Method for the cross-ply plate. Black circles denote the PZTs and the triangle shows damage located at coordinate (38 cm, 48 cm).

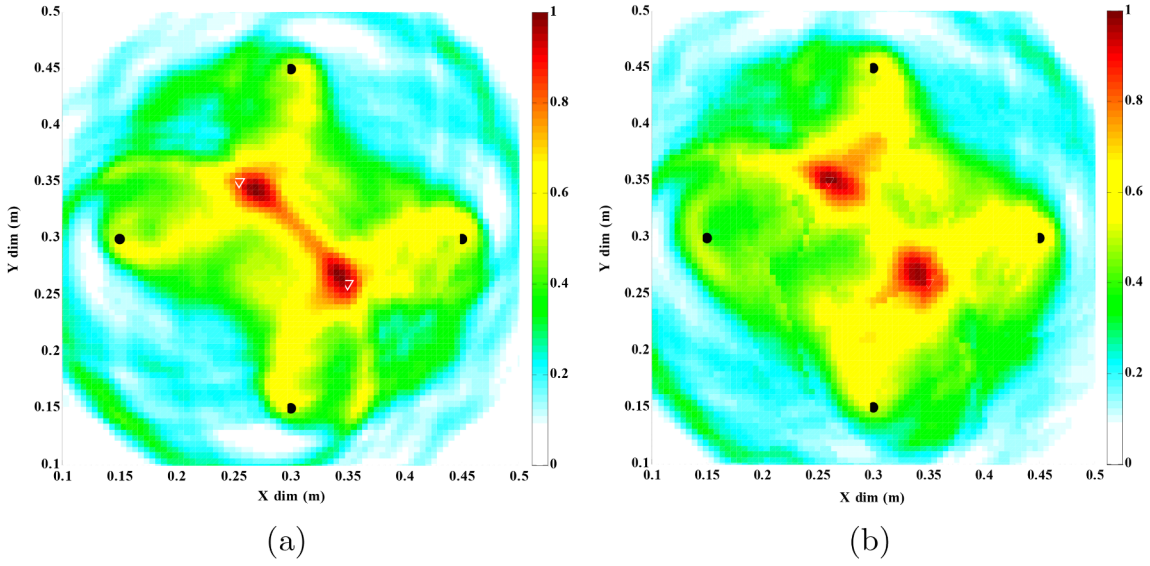

Fig. 16. Images reconstructed via (a) the conventional DAS method (b) the modified DAS Method for the quasi-isotropic plate. Black circles denote the PZTs and the triangles show damages located at coordinates (26 cm, 35 cm), (35 cm, 26 cm).

As it is impossible to have the wave velocity for all angles, we discretized 360° into 8 segments based on the direction of the measured wave velocities. Figs. 10 and 11 shows the polar plot of the group velocity of traveling wave at the different directions for the quasi-isotropic and cross-ply plates respectively for the given frequency.

4.2. Comparison of modified and conventional DAS and SR methods

In the conventional DAS and SR methods, the same wave velocity is used for all directions. It should be noted that, in the semi-isotropic plate, there is not a significant difference between the measured wave velocities for different directions, as shown in Table 2. However, in the cross-ply plate, the group velocity is direction-dependent more obviously than in the quasi-isotropic plate and in both cases this feature affects the accuracy of damage detection and location. Figs. 12–15 compare the damage location accuracy of the conventional and the modified DAS and SR methods in the presence of one simulated damage placed on the quasi-isotropic and cross-ply plates.

Also, Figs. 16–19 show the comparison between the results achieved by conventional and modified DAS and SR methods to locate two virtual damage locations on both the composite plates.

As it can be seen from Figs. 12–19, the accuracy of damage detection and location in the modified DAS and SR methods has been improved in comparison with the conventional DAS and SR methods in both the quasi-isotropic and the cross-ply plate. Although the comparison between these two cases (quasi-isotropic and cross-ply plates) is not fair due to the difference in virtual damage location, this qualitative comparison shows that the vulnerability of damage detection and location in the cross-ply plate is more than in the quasi-isotropic plate when the average wave velocity is used instead of the direction-dependent one.

4.3. Using the hybrid DAS-SR method

After using the modified DAS and SR methods, in the next step we combined these two methods and used the hybrid DAS-SR method to

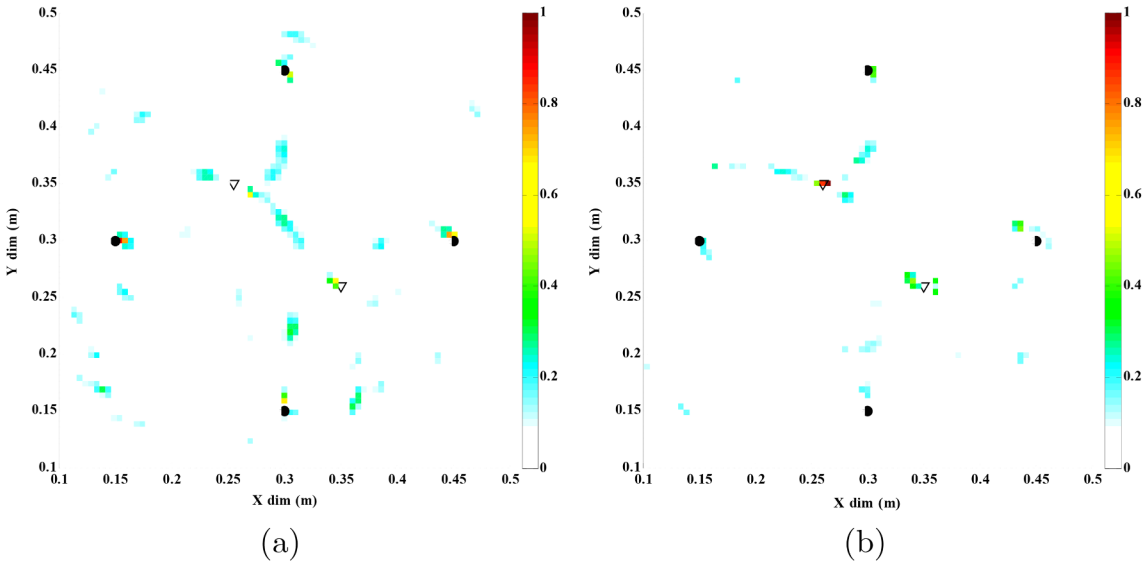

Fig. 17. Images reconstructed via (a) the conventional SR method (b) the modified SR Method for the quasi-isotropic plate. Black circles denote the PZTs and the triangles show damages located at coordinates (26 cm, 35 cm), (35 cm, 26 cm).

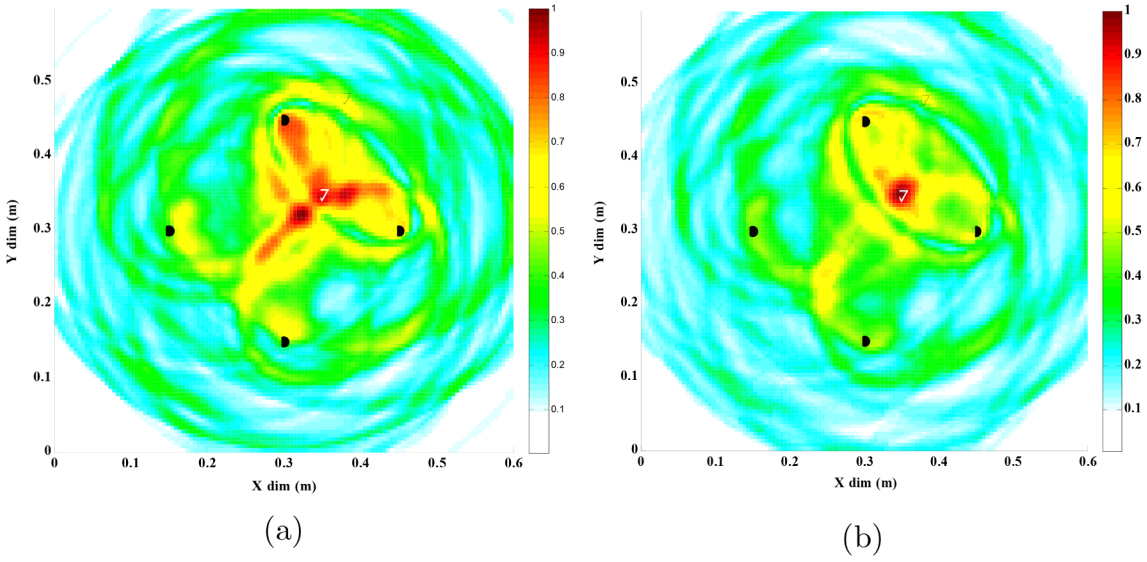

Fig. 18. Images reconstructed via (a) the conventional DAS method (b) the modified DAS Method for the cross-ply plate. Black circles denote the PZTs and the triangles show damages located at coordinates (38 cm, 48 cm), (35 cm, 35 cm).

increase the accuracy of detection and location of multi-virtual damages on both plates and the impact damage on the quasi-isotropic plate.

Figs. 20–22 show the comparison of the results obtained by modified DAS, SR and hybrid methods, for one, two, and three virtual damages respectively for the quasi-isotropic plate.

In Figs. 20(b) and 22 (b), it can be seen that some wrong detections have occurred in the SR method results. Also, Fig. 22(b) shows that the SR method could not detect the third virtual damage. In addition, the DAS results show a high noise level near the damage location and at some other points. Also, Figs. 23–25 show the comparison of the results obtained by modified DAS, SR and hybrid methods, for one, two, and three virtual damages placed on the cross-ply plate.

Fig. 24(b) shows that many wrong detections have occurred in the SR method results. Also, Fig. 25(b) shows that the SR method could not detect the third virtual damage. In addition, the DAS result depicted in Fig. 25(a) shows a high noise level in many area especially in the vicinity of damage locations.

At the next step the impact induced damage is studied. Fig. 26 shows the 11.2 J impacted damage location by modified DAS, SR and Hybrid methods.

As it can be seen from Fig. 26, in the DAS method if the spot size is too large, it is quite difficult to find the exact impact damage location. This could be even more challenging if the impact location is near to the boundaries of the plate or close to other scattering locations. Also, the image reconstructed by the SR method shows an error in the damage location and a wrong detection near PZT 2, however the hybrid method yields accurate results.

It is clear from Figs. 20–26 that the Hybrid method significantly improves the damage detection and location in comparison with both the DAS and SR methods when separately used.

5. Conclusion

In this study, two achievements were made in improving the damage detection-location applicability of the two conventional imaging

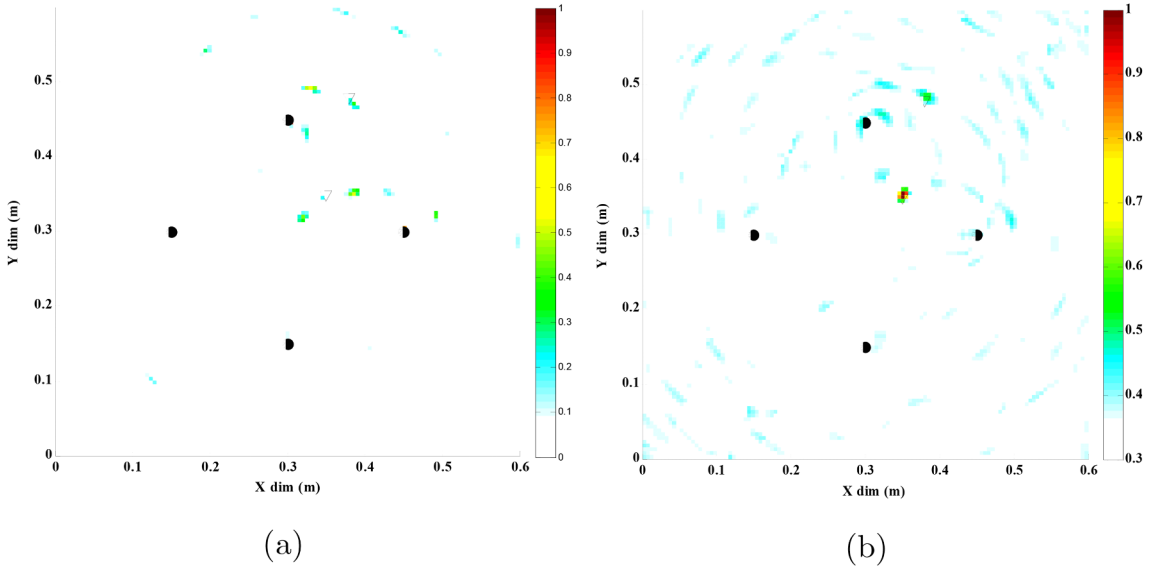

Fig. 19. Images reconstructed via (a) the conventional SR method (b) the modified SR Method for the cross-ply plate. Black circles denote the PZTs and the triangles show damages located at coordinates (38 cm, 48 cm), (35 cm, 35 cm).

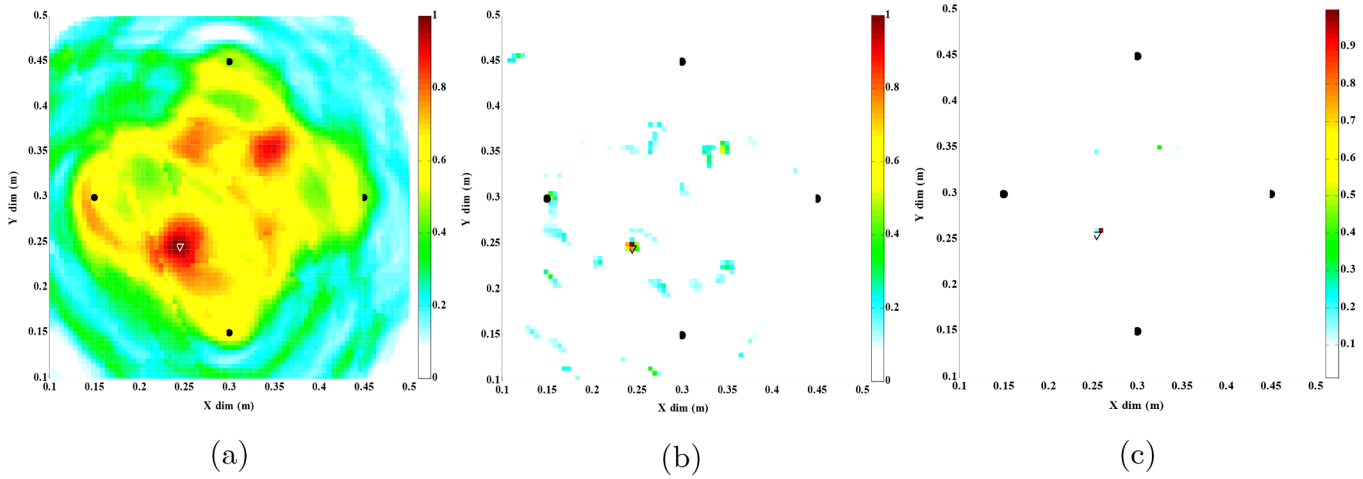

Fig. 20. Images reconstructed via (a) the modified DAS method, (b) the modified SR Method (c) the Hybrid method. Virtual damage is located at coordinate (25 cm, 25 cm).

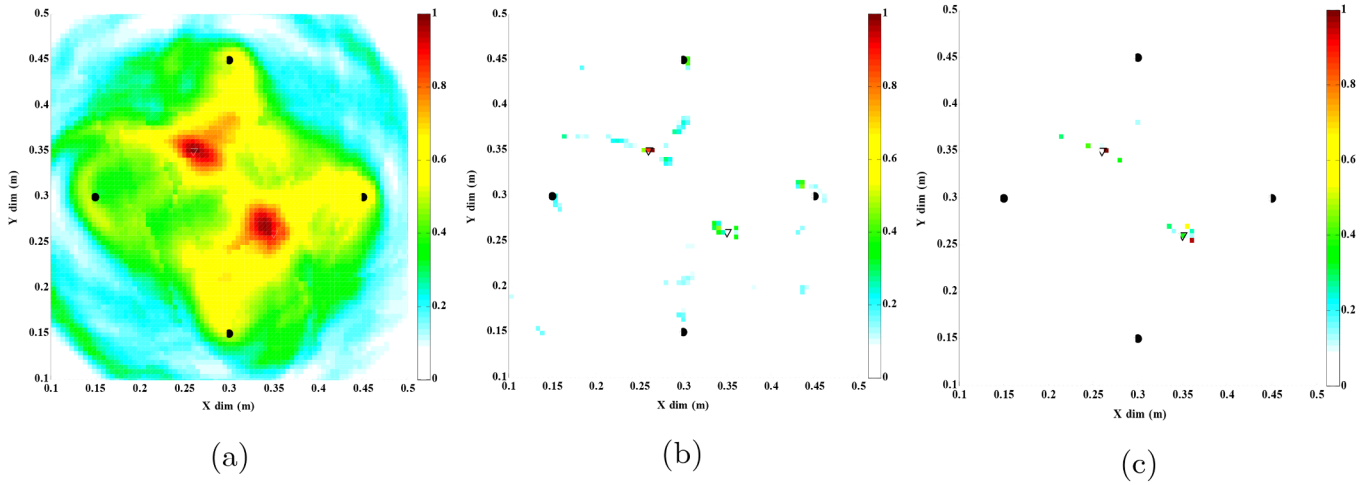

Fig. 21. Images reconstructed via (a) the modified DAS method, (b) the modified SR Method (c) the Hybrid method. Virtual damages are located at coordinates (26 cm, 35 cm), (35 cm, 26 cm).

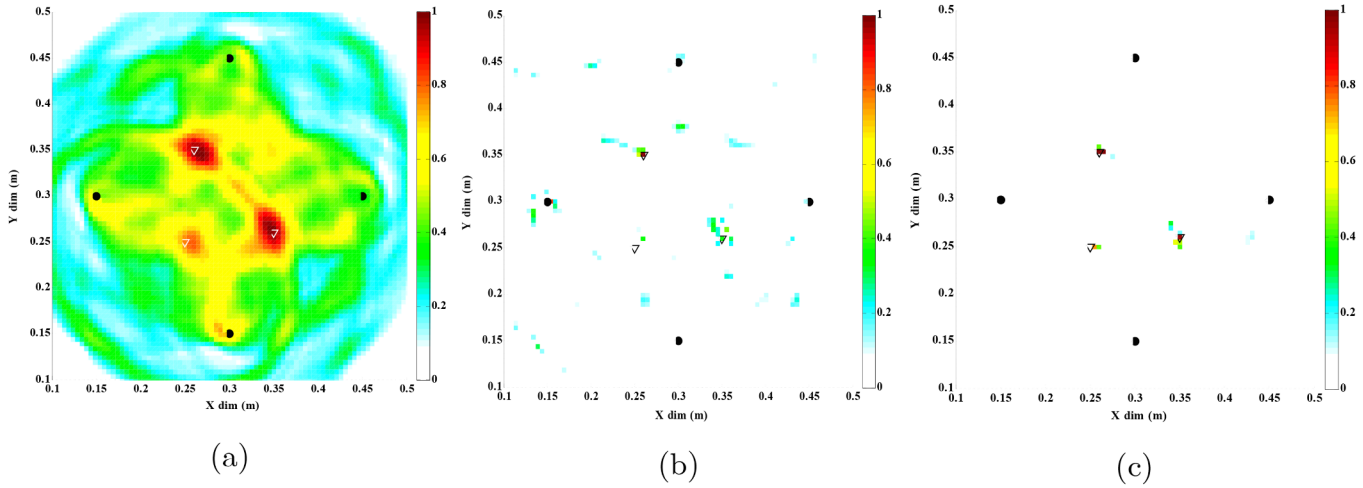

Fig. 22. Images reconstructed via (a) the modified DAS method, (b) the modified SR Method (c) the Hybrid method. Virtual damages are located at coordinates (26 cm, 35 cm), (35 cm, 26 cm) and (25 cm, 25 cm).

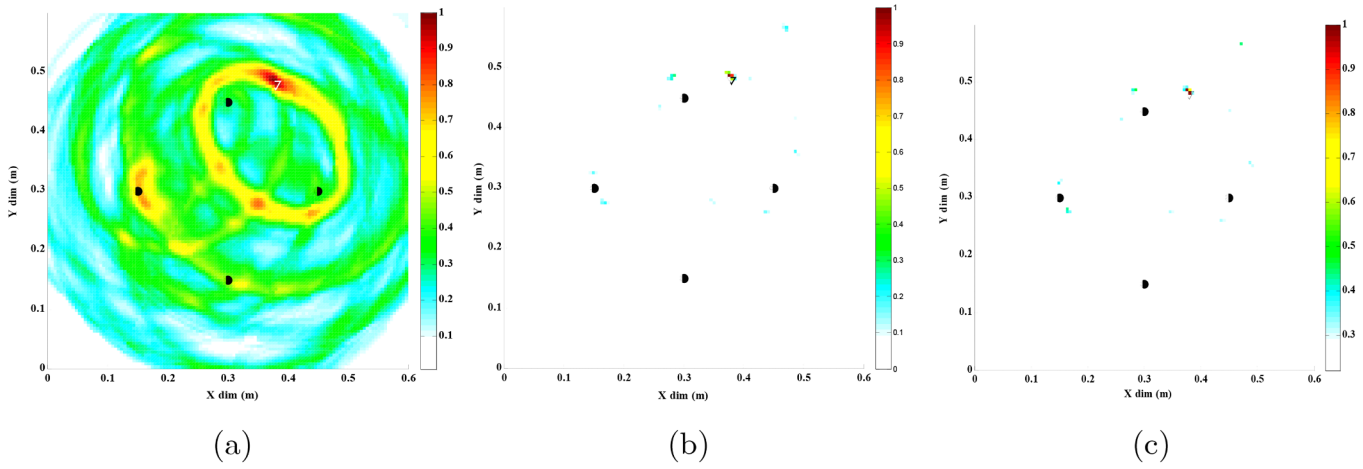

Fig. 23. Images reconstructed via (a) the modified DAS method, (b) the modified SR Method (c) the Hybrid method. Virtual damage is located at coordinate (38 cm, 48 cm).

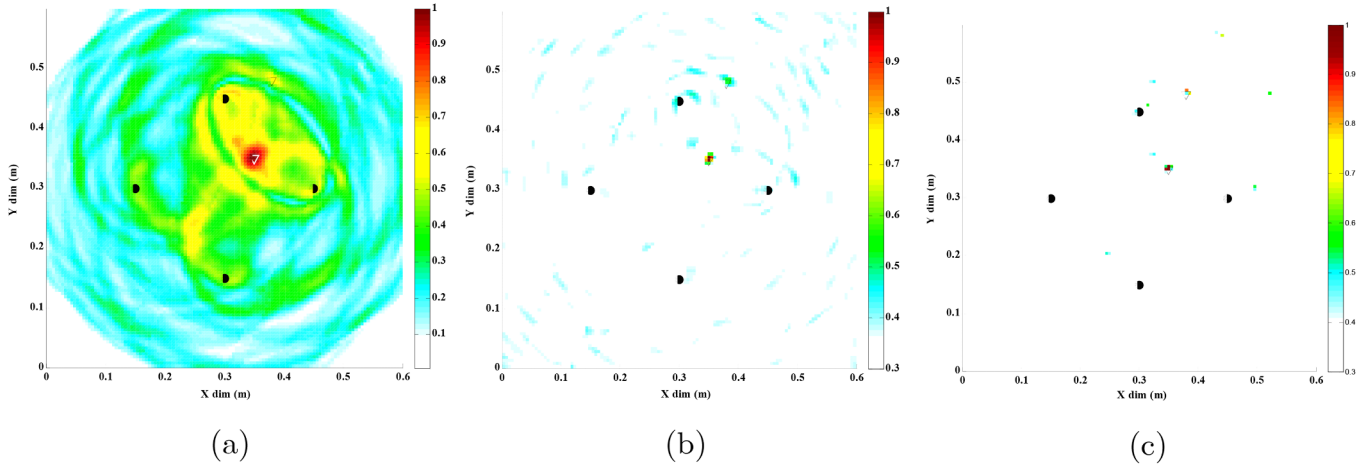

Fig. 24. Images reconstructed via (a) the modified DAS method, (b) the modified SR Method (c) the Hybrid method. Virtual damages are located at coordinates (35 cm, 35 cm), (38 cm, 48 cm).

methods for Structural Health Monitoring (SHM) of composite structures. At the first step the Sparse Reconstruction (SR) and the Delay-And-Sum (DAS) methods were modified to be suitable for assessing composite materials. To modify the SR method, in forming the dictionary matrix, the direction-dependent group velocity was used instead of a single global phase velocity. Also, the direction-dependent group velocity was used in the calculation of Time-of-Flight in the modified DAS method. Some experiments were performed on the quasi-

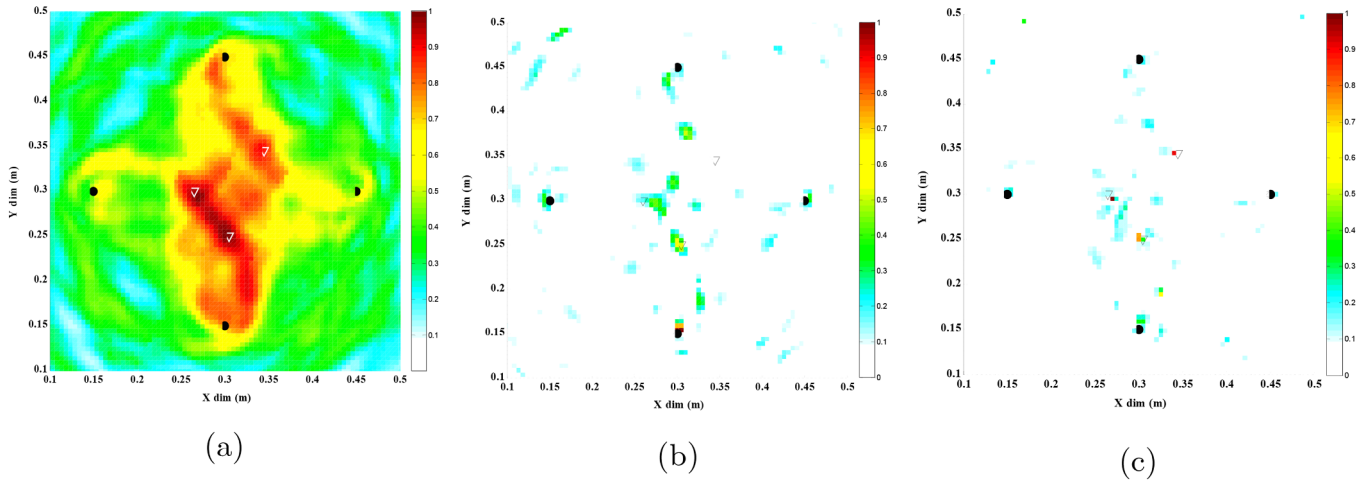

Fig. 25. Images reconstructed via (a) the modified DAS method, (b) the modified SR Method (c) the Hybrid method. Virtual damages are located at coordinates (25 cm, 30 cm), (30 cm, 25 cm) and (35 cm, 35 cm).

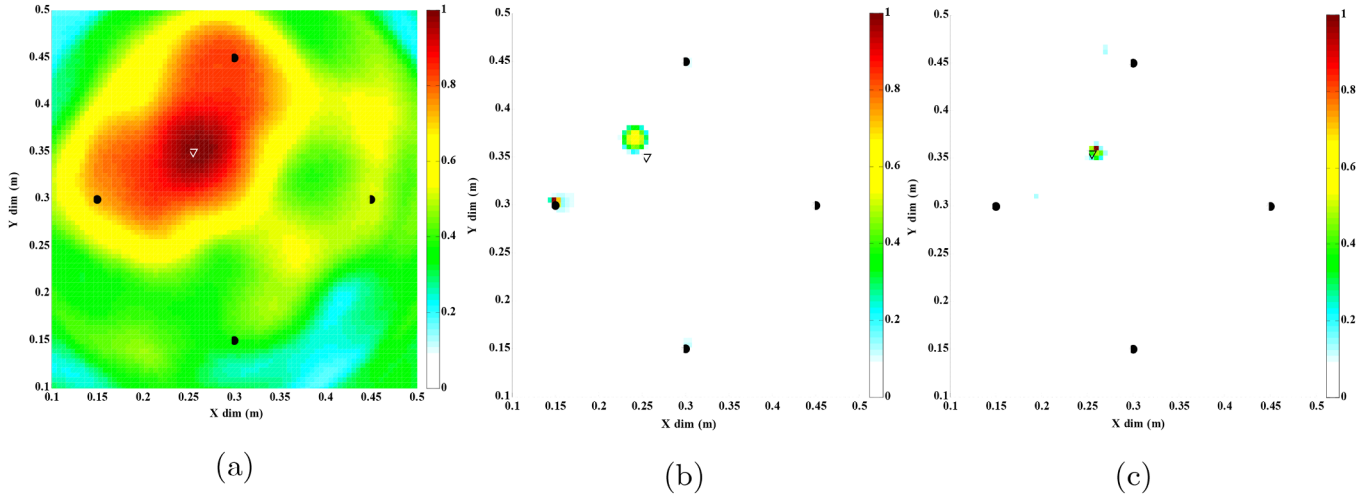

Fig. 26. Images reconstructed via (a) the modified DAS method (b) the modified SR Method (c) the Hybrid method. Impact damage is located at coordinate (25.5 cm, 35 cm).

isotropic and cross-ply composite plates, which show that this modification increased the accuracy of damage detection and localization in both composite plates for virtual damages. At the next step, the modified DAS and SR methods were combined and the hybrid DAS-SR method was assessed for its performance in detecting and locating multi-virtual damage locations as well as an experimental Barely Visible Impact Damage (BVID). The images reconstructed from the experimental measurement data show that the damage detection and localization capability of the hybrid method is significantly better than the DAS and SR methods when separately used.

Declaration of Competing Interest

The authors declare that they have no known competing financial interests or personal relationships that could have appeared to influence the work reported in this paper.

Acknowledgement

The authors would like to thank Mr. Jochem Frudiger, GTM Advanced Structures, for providing C-scan image of the impacted composite plate.

Appendix A. Supplementary data

Supplementary data to this article can be found online at https://doi.org/10.1016/j.compstruct.2020.112420.

References

[1] Giurgiutiu V. Structural health monitoring of aerospace composites. Academic Press; 2015.
[2] Tserpes KI, Karachalios V, Giannopoulos I, Prentzias V, Ruzek R. Strain and damage monitoring in CFRP fuselage panels using fiber Bragg grating sensors. Part I: design, manufacturing and impact testing. Compos Struct 2014;107:726–36.
[3] Soutis C, Beaumont PW, editors. Multi-scale modelling of composite material systems: the art of predictive damage modelling. Elsevier; 2005.
[4] Balageas D, Fritzen CP, Güemes A, editors. Structural health monitoring (Vol. 90). John Wiley & Sons; 2010.
[5] Levine R. Ultrasonic guided wave imaging via sparse reconstruction PhD Thesis Georgia Institute of Technology, USA; 2014.
[6] Maio L, Memmolo V, Ricci F, Boffa ND, Monaco E, Pecora R. Ultrasonic wave propagation in composite laminates by numerical simulation. Compos Struct 2015;121:64–74.
[7] Su Z, Ye L, Lu Y. Guided Lamb waves for identification of damage in composite structures: a review. J Sound Vib 2006;295(3–5):753–80.
[8] Kessler SS, Spearing SM, Soutis C. Damage detection in composite materials using Lamb wave methods. Smart Mater Struct 2002;11(2):269–78.
[9] Saravanos DA, Heyliger PR. Coupled layerwise analysis of composite beams with embedded piezoelectric sensors and actuators. J Intell Mater Syst Struct 1995;6(3):350–63.

[10] Sarvanos D, Birman V, Hopkins D. Detection of delaminations in composite beams using piezoelectric sensors. In: Adaptive Structures Forum; June 1994, p. 1754.
[11] Seale MD, Smith BT, Prosser WH. Lamb wave assessment of fatigue and thermal damage in composites. J Acoust Soc Am 1998;103(5):2416–24.
[12] Guo N, Cawley P. The interaction of Lamb waves with delaminations in composite laminates. J Acoust Soc Am 1993;94(4):2240–6.
[13] Prasad SM, Balasubramaniam K, Krishnamurthy CV. Structural health monitoring of composite structures using Lamb wave tomography. Smart Mater Struct 2004;13(5):N73.
[14] Leonard KR, Hinders MK. Lamb wave tomography of pipe-like structures. Ultrasonics 2005;43(7):574–83.
[15] Wilcox PD. Omni-directional guided wave transducer arrays for the rapid inspection of large areas of plate structures. IEEE Trans Ultrason Ferroelectr Freq Control 2003;50(6):699–709.
[16] Purekar AS, Pines DJ. Damage detection in thin composite laminates using piezoelectric phased sensor arrays and guided Lamb wave interrogation. J Intell Mater Syst Struct 2010;21(10):995–1010.
[17] Yu L, Tian Z. Guided wave phased array beamforming and imaging in composite plates. Ultrasonics 2016;68:43–53.
[18] Su Z, Ye L. Lamb wave propagation-based damage identification for quasi-isotropic CF/EP composite laminates using artificial neural algorithm: Part I-methodology and database development. J Intell Mater Syst Struct 2005;16(2):97–111.
[19] Tabian I, Fu H, Sharif Khodaei Z. A convolutional neural network for impact detection and characterization of complex composite structures. Sensors 2019;19(22):4933.
[20] Michaels TE, Michaels JE. Sparse ultrasonic transducer array for structural health monitoring. In: AIP Conference Proceedings, Vol. 700, No. 1; February 2004, p. 1468–75.
[21] Clarke T, Cawley P, Wilcox PD, Croxford AJ. Evaluation of the damage detection capability of a sparse-array guided-wave SHM system applied to a complex structure under varying thermal conditions. IEEE Trans Ultrason Ferroelectr Freq Control 2009;56(12):2666–78.
[22] Hall JS, Michaels JE. Minimum variance ultrasonic imaging applied to an in situ sparse guided wave array. IEEE Trans Ultrason Ferroelectr Freq Control 2010;57(10):2311–23.
[23] Wang CH, Rose JT, Chang FK. A synthetic time-reversal imaging method for structural health monitoring. Smart Mater Struct 2004;13(2):415.
[24] Ng CT, Veidt M. A Lamb-wave-based technique for damage detection in composite laminates. Smart Mater Struct 2009;18(7):074006.
[25] Clarke T, Simonetti F, Cawley P. Guided wave health monitoring of complex structures by sparse array systems: Influence of temperature changes on performance. J Sound Vib 2010;329(12):2306–22.
[26] Michaels JE. Detection, localization, and characterization of damage in plates with an in situ array of spatially distributed ultrasonic sensors. Smart Mater Struct 2008;17(3):035035.
[27] Levine R, Michaels JE. Block-sparse reconstruction and imaging for lamb wave structural health monitoring. IEEE Trans Ultrasonic, Ferroelectrics, Frequency Control 2014;61(6):1006–15.
[28] Sharif-Khodaei Z, Aliabadi MH. Assessment of delay-and-sum algorithms for damage detection in aluminium and composite plates. Smart Mater Struct 2014;23(7):075007.
[29] Bekas DG, Mendias MM, Sharif Khodaei Z, Karachalios E, Alonso FJ, Aliabadi FM. SHM of composite mono-stringer elements based on guided waves. Key Eng Mater 2020;827:464–9.
[30] Zeng L, Huang L, Lin J. Damage imaging of composite structures using multipath scattering Lamb waves. Compos Struct 2019;216:331–9.
[31] Levine RM, Michaels JE. Model-based imaging of damage with Lamb waves via sparse reconstruction. J Acoust Soc Am 2013;133(3):1525–34.
[32] Lamb H. On waves in an elastic plate. Proc. R. Soc. Lond. A 1917;93(648):114–28.
[33] Glushkov E, Glushkova N, Eremin A, Lammering R. Group velocity of cylindrical guided waves in anisotropic laminate composites. J Acoust Soc Am 2014;135(1):148–54.
[34] Wang L, Yuan FG. Group velocity and characteristic wave curves of Lamb waves in composites: modeling and experiments. Compos Sci Technol 2007;67(7–8):1370–84.
[35] Laboratory for active materials and smart structures (LAMSS). University of South Carolina college of engineering and computing, http://www.me.sc.edu/research/lamss/html/software.html; 2016 [accessed 3 December 2019].
[36] Nokhbatolfoghahai A, Navazi HM, Groves RM. Use of delay and sum for sparse reconstruction improvement for structural health monitoring. J Intell Mater Syst Struct 2019;30(18–19):2919–31.
[37] Mohimani H, Babaie-Zadeh M, Jutten C. A fast approach for overcomplete sparse decomposition based on smoothed l0-norm. IEEE Trans Signal Process 2008;57(1):289–301.
[38] Flinth A. Optimal choice of weights for sparse recovery with prior information. IEEE Trans Inf Theory 2016;62(7):4276–84.
[39] Needell D, Saab R, Woolf T. Weighted-minimization for sparse recovery under arbitrary prior information. Informa Inference: J IMA 2017;6(3):284–309.
[40] Colavita M, Bowler A, Zhang X, Irving PE. Adhesively bonded CFRP straps as fatigue crack growth retarders on AA2024-T3. In: Proceedings of SAMPE Conference 2006; 2006.